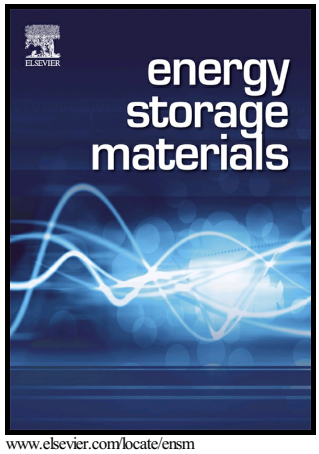

www.elsevier.com/locate/ensm

Hierarchical $NiCoO_2$ mesoprous microspheres as anode for lithium ion batteries with superior rate capability

Zhen-Dong Huang, Kun Zhang, Ting-Ting Zhang, Xu-Sheng Yang, Rui-Qing Liu, Yi Li, Xiu-Jing Lin, Xiao-Miao Feng, Yan-Wen Ma, Wei Huang

PII: S2405-8297(15)30091-X
DOI: http://dx.doi.org/10.1016/j.ensm.2016.01.001
Reference: ENSM32

To appear in: *Energy Storage Materials*

Received date: 27 November 2015
Revised date: 31 December 2015
Accepted date: 1 January 2016

Cite this article as: Zhen-Dong Huang, Kun Zhang, Ting-Ting Zhang, Xu-Sheng Yang, Rui-Qing Liu, Yi Li, Xiu-Jing Lin, Xiao-Miao Feng, Yan-Wen Ma and Wei Huang, Hierarchical $NiCoO_2$ mesoprous microspheres as anode for lithium ion batteries with superior rate capability, *Energy Storage Materials*, http://dx.doi.org/10.1016/j.ensm.2016.01.001

Hierarchical $NiCoO_2$ mesoprous microspheres as anode for lithium ion batteries with superior rate capability

Zhen-Dong Huang *,[‡] [a] Kun Zhang, [a, ‡] Ting-Ting Zhang, [a] Xu-Sheng Yang, [b] Rui-Qing Liu, [a] Yi Li, [a] Xiu-Jing Lin, [a] Xiao-Miao Feng, [a] Yan-Wen Ma *, [a] and Wei Huang [a,c]

[a] Key Laboratory for Organic Electronics & Information Displays and Institute of Advanced Materials, Nanjing University of Posts & Telecommunications, Nanjing, 210046, P.R.China.

[b] Department of Mechanical and Aerospace Engineering, The Hong Kong University of Science and Technology, Clear Water Bay, Kowloon, Hong Kong, China.

[c] Key Laboratory of Flexible Electronics (KLOFE) & Institute of Advanced Materials (IAM), Jiangsu National Synergistic Innovation Center for Advanced Materials (SICAM), Nanjing Tech University (Nanjing Tech), Nanjing 211816, PR China.

[‡] Dr. Zhen-Dong Huang and Mr. Kun Zhang contributed equally to this work.

*Email: hzd0506127@gmail.com (Z.D. Huang), iamywma@njupt.edu.cn (Y.W. Ma).

Abstract: Nanostructured materials with small particle size and large surface area exhibit excellent rate capability, however, their cyclic performances are normally limited by the intemperate side reaction with electrolyte, which is resulted from the large contact surface area of nanosized active particles with electrolyte. To avoid this issue, a relatively denser $NiCoO_2$ (NCO) hierarchical microspheres built by mesoporous thorn array are developed by pyrolyzing the agave-stricta-like $NiCo(OH)_2CO_3$ thorn microspheres under nitrogen gas in this work. The

analysed experimental results suggest that the hierarchical mesoporous nanostructure constructed by interconnected nanoparticles with a proper size (neither too small nor to large) shows a favourable BET specific surface area to well balance the rate and cyclic performance of transition metal oxide anodes. Compared to reported similar works, the as-prepared hierarchical NCO mesoprous microspheres deliver superior rate capability and greatly promoted cyclic stability, i.e. 844.6, 627.9 and 396.6 $mAhg^{-1}$ at 80, 1600 and 4000 mAg^{-1}, respectively.

Keywords: Nickel cobalt oxides; Hierarchical microsphere; Anode materials; Lithium ion batteries;

1. Introductions

Recent decades, the attractive characteristics, such as high energy density, cyclic stability and environmental benignity, make rechargeable lithium ion batteries (LIBs) become the dominant energy sources to power portable electronic devices, electric tools and electric vehicles, and the desirable energy stations to store the electric energy generated from solar and wind energy.[1] To satisfy ever-growing demands for large-scale and high power applications, the design and synthesis of novel hierarchical nanostructured high capacity electrode materials is one of the key approaches to promote the electrochemical properties, especially rate capability of LIBs.[1,2]

Anode, together with cathode and electrolyte, are three pivotal components of LIBs. The Li-ion storage properties of LIBs highly depend on the capacity, rate capability and cyclic stability of anode materials. [3] Nowadays, although traditionally carbonaceous materials still dominate the industrial anode market for their relatively better cyclic stability, their inherent low theoretical specific capacity of carbon (372 mAh g^{-1}) can't satisfy the future

high energy and high power applications of LIBs. [4] Owing to their much larger theoretical capacity and low cost, transition metal oxide (TMO) have been considered as one type of promising alternative anode material. [5-8] However, the poor rate and cyclic performance of TMOs, which are caused by the slow kinetics of electrochemical conversion reaction and the significant volumetric change during the charge/discharge process and other side reactions, remain to be further improved to satisfy the application requirements.

Single phase CoO, Co_3O_4 and NiO, i.e. porous CoO nanonets,[9] hierarchical Co_3O_4 peony-like microspheres, [10] NiO hollow nanospheres, [11] Yolk-Shell and cubic NiO nanopowder, [12] have been developed as promising high capacity anode materials with impressive improvements. Recently, binary transition metal oxides were thought to present synergistically enhanced electrical/ionic conductivity, reversible capacity, mechanical stability, which are superior to single phase metal oxides. Therefore, binary $ZnFe_2O_4$,[13] $ZnMn_2O_4$,[14] $ZnCo_2O_4$,[15, 16] $NiCo_2O_4$,[17] and $MnCo_2O_4$, [18-23] with different nanostructures have attracted intensive attention and been developed as advanced anode materials for LIBs. The entire electrochemical process can be classified as follows, take $NiCo_2O_4$ as example.[24]

$$NiCo_2O_4 + 8Li^+ + 8e^- \rightarrow Ni + 2Co + 4Li_2O \quad (1)$$

$$Ni + Li_2O \leftrightarrow NiO + 2Li^+ + 2e^- \quad (2)$$

$$Co + Li_2O \leftrightarrow CoO + 2Li^+ + 2e^- \quad (3)$$

$$CoO + 1/3Li_2O \leftrightarrow 1/3Co_3O_4 + 2/3Li^+ + 2/3e^- \quad (4)$$

According to this energy storage mechanisms, most of the reversible capacity of $NiCo_2O_4$ are ascribed to the reversible conversion reactions of NiO and CoO components, see

equation 2 and 3. In terms of above concerns, it is also great attractive to directly design $NiCoO_2$ with favorable nanostructures and investigate the electrochemical performance as anode materials for LIBs of nanostructured $NiCoO_2$. However, $NiCoO_2$ also suffers the same problems with $Ni_xCo_{3-x}O_4$, such as limited rate capability due to the slow electrochemical conversion kinetics and poor electric conductivity of $NiCoO_2$ and the poor cyclic performance resulted from the large volumetric change and continuous formation of solid electrolyte interphase during the charge/discharge cycles. Normally, graphene, carbon nanotube and other amorphous carbons can be introduced as conductive additives and substrates to improve the electronic conductivity and cyclic performance in a certain degree. [25-28] Except this, the capacity and slow kinetic of $NiCoO_2$ could be further enhanced through developing nanostructured materials to minimize the lithium ion transfer distance, nevertheless, the cyclic performance and density of nanostructured $NiCoO_2$ still should be further promoted by suppressing the intemperate side reaction with electrolyte through developing relatively denser nanostructure. For example, one-dimension hierarchical $NiCoO_2$ nanotube and $CoNiO_2$ microflowers assembled with nanosheets just reported by Xu et al and Liu et al, respectively, delivered a high capacity, but showed limited cyclic stability. [25, 29]

Therefore, this work focuses on improving the rate and cyclic performance of $NiCoO_2$ through developing novel nanostructured $NiCoO_2$ to achieve a balance between transfer distance for lithium ion and the exposed surface area for the formation of SEI film. Herein, a hierarchical agave-stricta-like $NiCoO_2$ microsphere built by mesoporous thorn array is newly developed by annealing the as-prepared nickel cobalt hydrocarbonate $NiCo(OH)_2CO_3$ thorn microsphere

precursor, which is self-assembled through a controllable and scalable hydrothermal method, under nitrogen atmosphere. Comparing to the reported nanotube and microflowers assembled with nanosheets, the agave-stricta-like sphere could reach a relatively higher compacted density, since the thorns formed by the interconnected $NiCoO_2$ nanoparticles could inserted into and fill the empty space of its neighboring spheres. Moreover, the mesoporous thorns formed by interconnected nano-sized particles endue the as-prepared agave-stricta-like $NiCoO_2$ microspheres with a short diffusion distance and favourable active area for Li^+, together with the suppressed side reaction with electrolyte. These should be the reasons we are exciting to find the as-prepared hierarchical $NiCoO_2$ microspheres built with nanoscale mesoporous thorn arrays exhibit superior rate capability and greatly promoted cyclic stability.

2. Experimental

2.1. Raw materials

In this work, urea (Purity ≥ 99%, Xilong Chemical Co., Ltd.), $NiCl_2·6H_2O$ (Purity ≥ 98%, Xilong Chemical Co., Ltd.), $CoCl_2·6H_2O$ (Purity ≥ 99%, Sinopharm Chemical Reagent Co.,Ltd) and distilled water were used as raw materials without further purification to prepare the precursor and final products $NiCoO_2$.

2.2. Synthesis of $NiCoO_2$ thorn spheres

In a typical preparation process, stoichiometric urea, $NiCl_2·6H_2O$, $CoCl_2·6H_2O$ in a molar ratio of 2/1/1 were firstly dissolved into 60 ml distilled water under vigorous magnetic stirring, respectively. Subsequently, the obtained clear mixed solution was transferred into a 100 ml Teflon container, and then sealed into a stainless steel autoclave. Thereafter, the sealed autoclave was put into a blowing dry box which had been pre-heated to 120 ^oC. To obtain the designed nanostructure, the self-assembling hydrothermal reaction was continuously carried out at 120 ^oC for 16h. After being washed with distilled water for 3 times, the obtained products were dried at 60 ^oC for 10h and collected as precursor for preparing the final product $NiCoO_2$. Finally, the final products of NCOs were obtained by annealing the precursor obtained above at a relatively low temperature

300, 350, 400, 450 and 500 ^{o}C for 2h under nitrogen gas atmosphere. The obtained $NiCoO_2$ were marked as NCO-300, NCO-350, NCO-400, NCO-450 and NCO-500, respectively.

2.3. Characterization

The morphology of as-prepared precursor and final products are characterized by using field emission scanning electron microscopy (FE-SEM, Hitachi S-4800) at an acceleration voltage of 15 kV and field emission transmission electron microscope (FE-TEM, JEOL 2010F) at an accelerating voltage of 200 kV. Nitrogen adsorption/desorption isotherms were obtained at 77 K using an automated adsorption apparatus (Micromerit-ics ASAP 2020). The surface area was calculated based on the Brunauer–Emmett–Teller (BET) equation. The X-ray diffraction patterns of as-prepared precursor and final products are measured on an X-ray diffractometer (RIGAKU, RINT-ULTIMA III) using Cu Kα radiation (λ= 1.54051Å). The diffraction patterns were recorded in the 2θ range of 10-80 ^{o} with a step size of 0.01 ^{o}. The crystal structure of NCOs were simulated by using the software of Materials Studio 6.0. The corresponding XRD pattern was calculated by following the reflux function of Materials Studio 6.0. The graphic representation of crystal structure was drawn by the software of VESTA.

In order to investigate the electrochemical performance of as-prepared NCO thorn spheres, the composite electrodes of NCOs were prepared by coating the uniform slurry of NCOs mixed with acetylene black (AB) and Polyvinylidenefluoride (PVDF) (NCO/C/PVDF=75/15/10). The electrode was then pressed and punched out into 10 mm disks in diameter. Two-electrode lithium ion batteries were assembled in an ultrapure Ar-gas filled glove box to study the lithium ion storage performance of NCOs in the electrolyte of 1 mol L^{-1} $LiPF_6$ in ethylene carbonate (EC) + dimethyl carbonate (DMC) + Ethyl methyl carbonate (EMC). Lithium discs were used as counter and reference electrodes. Cyclic voltammetry (CV) and galvanostatic charge and discharge measurements were carried out in the electrolytic window range of 0.02 to 3 V vs Li/Li^{+} at the scanning rate of 0.1 mVs^{-1} and at the current range of 80 - 4000 mA g^{-1}, respectively. The electrochemical impedance spectroscopy was measured in the frequency range from 100 kHz to 0.01 Hz, and the perturbation amplitude was controlled at 5 mV.

3. Results and discussions

3.1. Morphology and crystal structure of precursor

Fig. 1 presents the X-ray diffraction pattern and SEM images of the precursor self-assembled through a controllable and scalable hydrothermal method. As shown in Fig. 1a, the X-ray diffraction (XRD) pattern of precursors are matched well with that of reported monoclinic cobalt hydroxycarbonate, [9] which confirms that the self-assembled precursor is monoclinic binary $NiCo(OH)_2CO_3$. It is also very interesting to find that the obtained precursor has an agave-stricta-like morphology. The obtained hierarchical microspheres in ~ 4 - 8 μm are built by well-organized agave thorn arrays, see Figs. 1b and 1c.

3.2. Morphology and physical properties of as-prepared $NiCoO_2$

To prepare the target $NiCoO_2$ materials, the as-prepared $NiCo(OH)_2CO_3$ were heat treated at a low temperature (300 to 500 ^oC) for 2h under N_2 gas. The obtained samples were marked as NCO-300, NCO-350, NCO-400, NCO-450 and NCO-500, respectively. The XRD patterns of the corresponding NCOs, except NCO-300, are indexed to a pure cubic phase $NiCoO_2$, which is similar with NiO phase (JCPDS no. 65-2901), see Fig. 2a. This observation indicates that most of $NiCo(OH)_2CO_3$ have been decomposed when the calcination temperature is above 350 ^oC, and in turn transform to binary $NiCoO_2$. As graphic representation in Fig. 2b, the Co^{2+} and Ni^{2+} randomly located in 4a site of the NaCl-type cubic structure of $NiCoO_2$. The simulated XRD pattern, refluxed from the cubic structure in Fig. 2b, is similar with the observed pattern of NCO-500, see Fig. 2a. Due to the broadening effect of nanosize particles, the slight peak splitting of the calculated $NiCoO_2$ is difficult to be distinguished from the experimentally observed XRD patterns, see Fig. 2a. Fig. 3 present the high-resolution transmission electron microscope (HRTEM)

images, Fourier-filtered image and fast Fourier transformation (FFT) images corresponding to the selected area outlined by dashed red line of NCO-350 in Fig. 3a. The high resolution lattice fringe of selected area presented in Fig. 3b and 3c within the lattice spacing of ~0.244 nm and ~0.149 match well with the (111) and (220) plane of cubic phase NiO (JCPDS no. 65-2901). What is more, the corresponding (FFT) patterns of the selected area is also clear regular diffraction spots of cubic phase NiO, see Figs. 3d. All above observation suggests that the obtained NCOs nanoparticles are comprised of single crystal $NiCoO_2$.

The SEM images, see Figs. 4, indicate that the agave-strictanana-like morphology is still maintained even after being calcined at the temperature from 350 to 500 ^oC. However, the monolithic $NiCo(OH)_2CO_3$ thorns become porous thorns integrated by nanosized NCO particles due to the generation of large amount of CO_2 and H_2O gas when $NiCo(OH)_2CO_3$ decomposes during the calcination process, as illustrated in Fig. 5. Finally, the agave-stricta-like hierarchical NCO spheres formed with mesoporous thorn array were obtained. The average sizes of the obtained primary oxide particles grow from ~10 to ~50 nm, see the TEM images in Fig. 6. The nitrogen adsorption/desorption isotherm and pore-size distribution curves present in Fig. 7 confirm the mesoporous characteristics of NCOs thorn spheres. The calculated BET specific surface area of NCO-350, NCO-400, NCO-450 and NCO-500 were about 47, 27, 16 and 16 m^2g^{-1}, respectively. The average pore size of NCOs increased from ~ 8 to ~30 nm with the increase of calcination temperature from 350 ^oC to 500 ^oC, see Fig. 7c. Nevertheless, the Acquire HAADF image and corresponding EDX mapping for O, Co and Ni, shown in Fig. 8, indicate that all NCOs have uniform compositions, which also supports the formation of single phase $NiCoO_2$ observed in

XRD.

3.3. Lithium ion storage behaviours of as-prepared $NiCoO_2$

To better understand the electrochemical behavior of as-prepared NCOs, the cyclic voltammetry (CV) and electrochemical impedance spectroscopy (EIS) were carried out in this work. Figs. 9a and 9b show typical CV curves of the initial and third cycle of NCOs, respectively. As can be seen, there are well-defined sharp oxidation peaks at 1.6/2.25 V, derived from the oxidation of Ni^0 to Ni^{2+} and Co^0 to Co^{2+}. [28] In addition, a single primary reduction peak at approximately 0.3 V in the first cathodic scan was observed, corresponding to the initial reduction of NiO−CoO to metallic Ni−Co, the irreversible formation of a solid−electrolyte interface (SEI) layer, and the decomposition of electrolyte. It can be found that NCO-400, -450 and -500 showed similar electrochemical activity, but better than that of NCO-350. After the first cycle activation, the potentials of the oxidation peaks at 2.25 V slightly shift to 2.36 V in the subsequent cycles, while the reduction peak becomes weak and shifts to 1.0 V (NCO-350 and -400) and 1.13 (NCO-450) and 1.17 (NCO-500). The large peak current and narrow voltage gap between reduction and oxidation peaks indicate that NCO-500 shows better electrochemical activity than other samples. Moreover, the charge transfer resistance of NCOs significantly decrease after the activation, see Figs. 9c and 9d. The charge transfer resistance of NCO-350, NCO-400, NCO-450 and NCO-500 gradually increase from ~42 to 97 Ω with the growth of primary particle size of NCOs.

Benefited from the nature of nano-sized primary particles and mesoporous hierarchical structure, which could provide short diffusion distance and proper active area for Li^+, all as-prepared NCOs delivered super rate performance, see Fig. 10. The initial specific discharge and charge capacities of NCO-400 are 1308 and 782 $mAhg^{-1}$ at the current density of 1600 mAg^{-1}, respectively. The

charge capacity of NCOs slightly decreased with the increment of synthesis temperature. Figs. 10a and 10b display the cyclic performance of all as-prepared NCOs tested at the constant current density of 1600 and 4000 mAg^{-1}, respectively. The obtained results shown in Fig. 10a and 10b indicate that NCO-350 and NCO-400 show higher rate performance than NCO-450 and NCO-500, however, both NCO-450 and NCO-500 deliver much better cyclic stability than NCO-350, and NCO-4 NCO-40050. The capacity retention ratio of NCO-500 were 55% and 37% at 1600 and 4000 mAg^{-1}, respectively. All above observation is consistent with the CV and EIS analysis results. Compared with the reported neat $NiCoO_2$ nanotube, [25] NiO-CoO nanosphere [28] and hierarchical $CoNiO_2$ mesoporous microflower, [29] NCO-500 delivers significantly cyclic stability, see Table 1. The great promoted cyclic stability should be profited from the effectively suppressed side reaction due to the decreased contact specific surface area with electrolyte. Meanwhile, due to the large volume expansion, the formed SEI film is not stable during the charge/discharge cycles. Thus, the Coulombic efficiency of NCOs are not high, especially during the initial cycle, but, the Coulombic efficiency of NCOs gradually increase with the decrease of contact surface area with electrolyte. As present in Fig. 10c and 10d, the Coulombic efficiency of NCO-500 could be stabilized at ~ 99% after about 10 cycles. The specific charge capacity of NCO-500 are 844.6, 790.4, 677.2, 627.9 and 396.6 $mAhg^{-1}$ at 80, 160, 800, 1600 and 4000 mAg^{-1}, respectively. After cycled at different current densities for 31 cycles, the discharge and charge capacity recovered to 945.3 and 916.9 $mAhg^{-1}$ at 80 mAg^{-1}, see Fig. 9d. Therefore, compared to the reported work, the as-prepared hierarchical nanostructured NCO spheres formed with mesoporous thorn array delivered much higher rate capability than that of reported neat $NiCoO_2$ nanotubes composed of nanosheets NiO-CoO nanosphere and hierarchical $CoNiO_2$ mesoporous microflower, as present in

Table 1. [25] Above results speak volume for that hierarchical nanostructures with favourable specific surface area and pore structure is good for achieving superior rate capability and great promoted cyclic stability.

Similar with previous reports, the voltage profiles shown in Fig. 10c could be attributed to the reduction of Ni^{2+} and Co^{2+} to metallic Ni and Co. The redox reaction of this electrochemical process for NCO-500 is believed to proceed as follows:

$$NiCoO_2 + 4Li^+ + 4e \rightarrow Ni + Co + 2Li_2O \quad (5)$$

Subsequently, when the tested batteries are discharged to a voltage lower than 0. 4V in this initial cycle, a catalytic side reaction between metallic Ni, Co and electrolyte can be commonly observed in first discharge process of NCOs. As a results of the catalytic side reactions, the solid electrolyte interface (SEI) film and organic polymeric/gel-like layer could be formed on the surface of active materials by electrolyte decomposition. [24, 30] This complex side reaction normally accounts for the large irreversible capacity and low coulombic efficiency. However, the partially reversible reduction and oxidation of electrolyte can be ascribed to the part of capacity over theoretical capacity (716.5 $mAhg^{-1}$) of $NiCoO_2$. [9]

4. Conclusions

In this work, hierarchical $NiCoO_2$ (NCO) microspheres built by mesoporous thorn array were obtained by pyrolyzing the hydrothermally assembled agave-strictanana-like $NiCo(OH)_2CO_3$ microspheres under nitrogen gas. The mesoporous structure of NCO thorns were created during the degassing process of CO_2 and H_2O gas from the decomposing $NiCo(OH)_2CO_3$ thorn arrays. The calculated BET specific surface area of

NCOs were 46.756, 26.8, 16.451 and 15.765 m^2g^{-1} in the ascending of synthesis temperature from 350 to 500 ^oC, respectively. For the hierarchical mesoporous nanostructures and the favourable BET specific surface area, NCO-500 microspheres prepared at 500 ^oC delivered superior rate capability and greatly promoted cyclic stability, i.e. 844.6, 627.9 and 396.6 $mAhg^{-1}$ at 80, 1600 and 4000 mAg^{-1}, respectively. Prospectively, the rate capability and cyclic stability could be further promoted by carbon coating or hybrid with graphene or CNTs in future.

Acknowledgements

This work was supported by National Natural Science Foundation of China (51402155), Priority Academic Program Development of Jiangsu Higher Education Institutions（PAPD）(YX03001), Jiangsu National Synergistic Innovation Center for Advanced Materials (SICAM), Foundation of NJUPT (NY214021).

References

[1] C.Z. Yuan, H. B. Wu, Y. Xie, X. W. Lou, Mixed Transition-Metal Oxides: Design, Synthesis, and Energy-Related Applications. Angew. Chem. Int. Ed., 2014, 53, 1488.

[2] D.W.Xu, Y.B. He, X.D. Chu, Z.J. Ding, B.H. Li, J.F. He, H.D. Du, X.Y. Qin and F.Y. Kang, Synthesis of Lithium Iron Phosphate/Carbon Microspheres by Using Polyacrylic Acid Coated Iron Phosphate Nanoparticles Derived from Iron(III) Acrylate. ChemSusChem, 2015, 8, 1009.

[3] L. Yu, L. Zhang, H. B. Wu, G.Q. Zhang and X. W. Lou, Controlled synthesis of hierarchical $Co_xMn_{3-x}O_4$ array micro-/nanostructures with tunable morphology and composition as integrated electrodes for lithium-ion batteries. Energy Environ. Sci., 2013, 6, 2664.

[4] Y. S. Luo, J. S. Luo, W. W. Zhou, X. Y. Qi, H. Zhang, Denis Y. W. Yu, C. M. Li, H. J. Fan, T.

Yu, Controlled synthesis of hierarchical graphene wrapped TiO_2@Co_3O_4 coaxial nanobelt arrays for high-performance lithium storage, J. Mater. Chem. A, 2013, 1, 273.

[5] S. Li, X.Y. Qin, H.R. Zhang, J.X. Wu, Y.B. He, B.H. Li, F.Y. Kang, Silicon/carbon composite microspheres with hierarchical core–shell structure as anode for lithium ion batteries. Electrochem. Commun., 2014, 49, 98.

[6] X.Y. Zheng, W. Lv, Y.B. He, C. Zhang, W.Wei, Y. Tao, B.H. Li, and Q. H. Yang, 3D Hollow Sn@Carbon-Graphene Hybrid Material as Promising Anode for Lithium-Ion Batteries. Journal of Nanomaterials, 2014, 2014, http://dx.doi.org/10.1155/2014/974285.

[7] B. Zhang, Y. Yu, Z.D. Huang, Y.B. He, D. Jang, W.S. Yoon, Y.W. Mai, F.Y. Kang and J.K. Kim, Exceptional electrochemical performance of freestanding electrospun carbon nanofiber anodes containing ultrafine SnO_x particles. Energy Environ. Sci., 2012, 5, 9895.

[8] B. Zhang, Q. B. Zheng, Z. D. Huang, S.W. Oh, J.K. Kim, SnO_2–graphene–carbon nanotube mixture for anode material with improved rate capacities. Carbon, 2011, 49, 4524.

[9] X.L. Zhou, Y.R. Zhong, M. Yang, Q. Zhang, J.P. Wei, and Z. Zhou, $Co_2(OH)_2CO_3$ Nanosheets and CoO Nanonets with Tailored Pore Sizes as Anodes for Lithium Ion Batteries. ACS Appl. Mater. Interfaces, 2015, 7, 12022.

[10] H.W. Che, A.F. Liu, S.X. Liang, X.L. Zhang, J.B. Mu, Y.M. Bai, J.X. Hou, Facile synthesis of three-dimensional hierarchical Co_3O_4 peony-like microspheres and their lithium storage performance. Superlattices and Microstructures, 2015, 83, 538.

[11] M. Sasidharan, N. Gunawardhana, C. Senthil and M. Yoshio, Micelle templated NiO hollow nanospheres as anode materials in lithium ion batteries. J. Mater. Chem. A, 2014, 2, 7337.

[12] S. H. Choi and Y. C. Kang, Ultrafast Synthesis of Yolk-Shell and Cubic NiO Nanopowders

and Application in Lithium Ion Batteries. ACS Appl. Mater. Interfaces, 2014, 6, 2312.

[13] L.R. Hou , L. Lian, L.H. Zhang , G. Pang , C.Z Yuan , and X.G. Zhang, Self-Sacrifi ce Template Fabrication of Hierarchical Mesoporous Bi-Component-Active ZnO/$ZnFe_2O_4$ Sub-Microcubes as Superior Anode Towards High-Performance Lithium-Ion Battery. Adv. Funct. Mater. 2014, DOI:10.1002/adfm.201402827.

[14] L.H. Zhang, S.Q. Zhu, H. Cao, G. Pang, J.D. Lin, L.R. Hou, C.Z. Yuan, Ultrafast spray pyrolysis fabrication of a nanophase $ZnMn_2O_4$ anode towards high-performance Li-ion batteries. RSC Adv., 2015,5, 13667.

[15] L.Y. Guo, Q. Ru, X. Song, S.J. Hu and Y.D. Mo, Pineapple-shaped $ZnCo_2O_4$ microspheres as anode materials for lithium ion batteries with prominent rate performance. J. Mater. Chem. A, 2015, 3, 8683.

[16] Y.Q. Zhu, C.B. Cao, J.T. Zhang and X.Y. Xu, Two-dimensional ultrathin $ZnCo_2O_4$ nanosheets: general formation and lithium storage application. J. Mater. Chem. A, 2015, 3, 9556.

[17] J.B. Cheng, Y. Lu, K.W. Qiu, H.L. Yan, J.Y. Xu, L. Han, X.M. Liu, J.S. Luo, J.K. Kim, Y.S. Luo, A novel $NiCo_2O_4$ anode morphology for lithium-ion batteries. Scientific Reports, 2015, 5, 12099, DOI:10.1038/srep12099.

[18] M.H. Kim, Y. J. Hong and Y. C. Kang, Electrochemical properties of yolk–shell and hollow CoMn2O4 powders directly prepared by continuous spray pyrolysis as negative electrode materials for lithium ion batteries. RSC Adv., 2013, 3, 13110.

[19] L.J. Wang, B. Liu, S.H. Ran, L.M. Wang, L.N. Gao, F.Y. Qu, D. Chen and G.Z. Shen, Facile synthesis and electrochemical properties of $CoMn_2O_4$ anodes for high capacity lithium-ion batteries. J. Mater. Chem. A, 2013, 1, 2139.

[20] Y.R. Liu, B.C. Zhang, J.K. Feng, and S.L. Xiong, General Formation of Mn-based Transition Metal Oxide Twin-Microspheres with Enhanced Lithium Storage Properties. RSC Adv., 2015, 5, 26863.

[21] L. Zhou, D.Y. Zhao, and X. W. Lou, Double-Shelled $CoMn_2O_4$ Hollow Microcubes as High-Capacity Anodes for Lithium-Ion Batteries. Adv. Mater., 2012, 24, 745.

[22] S. M. Hwang, S.Y. Kim, J.G. Kim, K.J. Kim, J.W. Lee, M.S. Park, Y.J. Kim, M. Shahabuddin, Y. Yamauchi and J.H. Kim, Electrospun manganese-cobalt oxide hollow nanofibers synthesized via combustion reactions and their lithium storage performance. Nanoscale, Nanoscale, 2015, 7, 8351.

[23] C.C. Fu, G.S. Li, D. Luo, X.S. Huang, J. Zheng, and L.P. Li, One-Step Calcination-Free Synthesis of Multicomponent Spinel Assembled Microspheres for High-Performance Anodes of Li-Ion Batteries: A Case Study of $MnCo_2O_4$, ACS Appl. Mater. Interfaces 2014, 6, 2439.

[24] J. F. Li, S. L. Xiong, Y. R. Liu, Z. C. Ju, Y. T. Qian, High Electrochemical Performance of Monodisperse NiCo2O4 Mesoporous Microspheres as an Anode Material for Li-Ion Batteries. ACS Appl. Mater. Interfaces, 2013, 5, 981–988.

[25] X. Xu, B.T. Dong, S.J. Ding, C.H. Xiao and D.M. Yu, Hierarchical $NiCoO_2$ nanosheets supported on amorphous carbon nanotubes for high-capacity lithium-ion batteries with long cycle life. J. Mater. Chem. A, 2014, 2, 13069.

[26] W. Lv, Z. Li, Y. Deng, Q. H.Yang, F.Y. Kang. Graphene-based materials for electrochemical energy storage devices: Opportunities and challenges. Energy Storage Materials, 2015, doi:10.1016/j.ensm.2015.10.002.

[27] F. Xiang, R. Mukherjee , J. Zhong, Y. Xia, N. Gu, Z. Yang, N. Koratkar. Scalable and rapid

Far Infrared reduction of graphene oxide for high performance lithium ion batteries. Energy Storage Materials, 2015, 1, 9-16.

[28] Y.H. Wei, F.L. Yan, X. Tang, Y.Z. Luo, M. Zhang, W.F. Wei, and L.B. Chen, Solvent-Controlled Synthesis of NiO−CoO/Carbon Fiber Nanobrushes with Different Densities and Their Excellent Properties for Lithium Ion Storage. ACS Appl. Mater. Interfaces 2015, 7, 21703−21711.

[29] Y. Liu, Y. Zhao, Y. Yu, M. Ahmad, H Sun. Facile synthesis of single-crystal mesoporous $CoNiO_2$ nanosheets assembled flowers as anode materials for lithium-ion batteries. Electrochimica Acta, 2014, 132, 404-409.

[30] F. F. Wu, C. H. Yu, W. X. Liu, T. Wang, J. K. Feng, S. L. Xiong, Large-scale synthesis of $Co_2V_2O_7$ hexagonal microplatelets under ambient conditions for highly reversible lithium storage, J. Mater. Chem. A, 2015, 3, 16728–16736.

Table captions

Table 1. Summary of the electrochemical performance of nanostructured $NiCoO_2$ reported in this and similar works.

Figure captions

Fig. 1. The X-ray diffraction pattern (a) and SEM image (b) of as-prepared precursors $NiCo(OH)_2CO_3$

Fig. 2. (a) The XRD patterns of NCO-300, NCO-350, NCO-400, NCO-450, NCO-500 and the calculated NiCoO2, respectively, (b) The 3D graphical crystal structure representation of NiCoO2.

Fig. 3. The high resolution TEM image of NCO-350 (a), Fourier-filtered image (b, c) and FFT image (d) from the selected area outlined by dashed red line in (a).

Fig. 4. The SEM images of the as-prepared NCO-350 (a), NCO-400 (b), NCO-450 (c), and NCO-500 (d), respectively.

Fig. 5. The Schematic illustration of the pyrolysis process of agave-stricta-like $NiCo(OH)_2CO_3$ (a) to prepare mesoporous $NiCoO_2$ spheres (b).

Fig. 6. The high resolution TEM images of the as-prepared NCO-350 (a), NCO-400 (b), NCO-450 (c), and NCO-500 (d), respectively.

Fig. 7. The nitrogen adsorption/desorption isotherm (a) and the Brunauer–Emmett–Teller (BET) specific surface area (b) and the pore-size distribution curve (c) and the pore volume (d) of hierarchical $NiCoO_2$ mesoporous spheres varied with the calcination temperatures.

Fig. 8. Acquire HAADF image and corresponding EDX mapping for O, Co and Ni of NCO-350 (a), NCO-400 (b), NCO-450 (c) and NCO-500 (d), respectively.

Fig. 9. The initial cycle (a) and the third cycle (b) cyclic voltammetry curve and the

electrochemical impedance spectroscopy before cycle (c) and after three CV cycles (d) at 0.1 mVs^{-1} of NCO-350, NCO-400, NCO-450 and NCO-500.

Fig. 10. The cyclic performance of NCO-350, NCO-400, NCO-450 and NCO-500 at 1600 mAg^{-1} (a) and 4000 mAg^{-1} (b); and the typical charge/discharge profile (c) and rate capability (d) of NCO-500 at the constant current densities from 80 mAg^{-1} to 4000 mAg^{-1}.

Table 1. Summary of the electrochemical performance of nanostructured $NiCoO_2$ reported in this and similar works.

Materials	Methods	Current (mAg^{-1})	Capacity ($mAhg^{-1}$)	Capacity retention (%)
Hierarchical mesoporous microspheres of this work	Hydrothermal self-assembly	400	~770	
		800	~677	
		1600	**~628**	**55% (50 cycle)**
		4000	~397	
$NiCoO_2$ nanotubes formed with nanosheets Ref. [25]	Amorphous carbon nanotube templated soft chemical method	**200**	**~1130**	**55.8 (50 cycle)**
		400	~600	
		800	~300	
NiCoO2@CNT Composites Ref. [25]		**200**	**~1150**	**110 (50 cycle)**
		400	~1100	
		800	~920	
NiO-CoO / carbon fiber nanobrushes Ref. [28]	Carbon fiber templated solvothermal strategy	**200**	**~1250**	**106 (50 cycle)**
		500	~900	
		1000	~600	
		2000	~300	
NiO-CoO nanospheres Ref. [28]	Hydrothermal method	**200**	**~1100**	**22 (50 cycle)**
mesoporous $CoNiO_2$ hierarchical microflowers Ref. [29]	Hydrothermal method	**100**	**~600**	**65 (50 cycle)**
		500	~300	
		1000	~200	

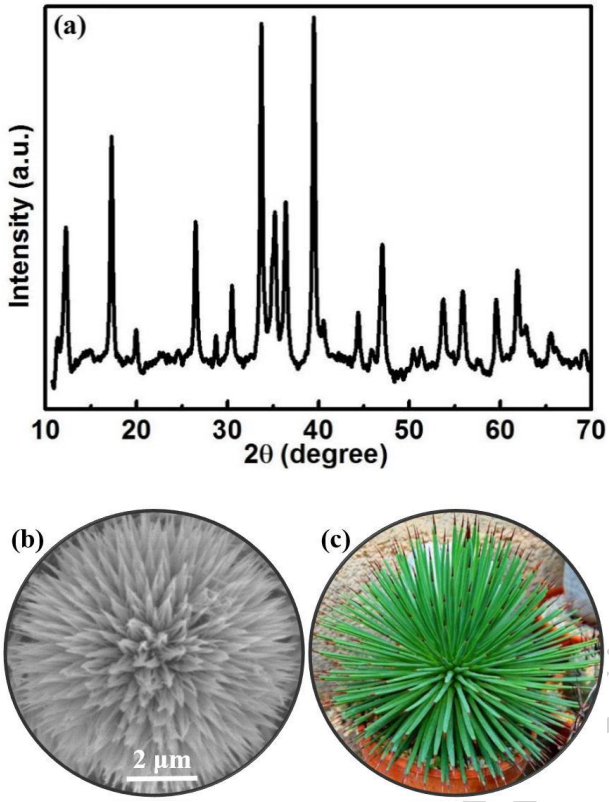

Fig. 1. The X-ray diffraction pattern (a) and SEM image (b) of as-prepared precursors $NiCo(OH)_2CO_3$ and (c) the optical picture of agave-strictanana.

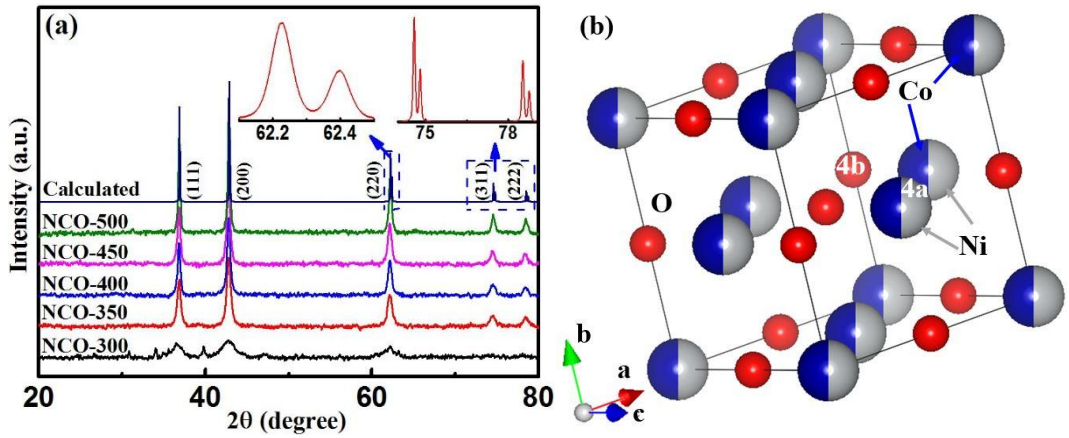

Fig. 2. (a) The XRD patterns of NCO-300, NCO-350, NCO-400, NCO-450, NCO-500 and the calculated $NiCoO_2$, respectively, (b) The 3D graphical crystal structure representation of $NiCoO_2$.

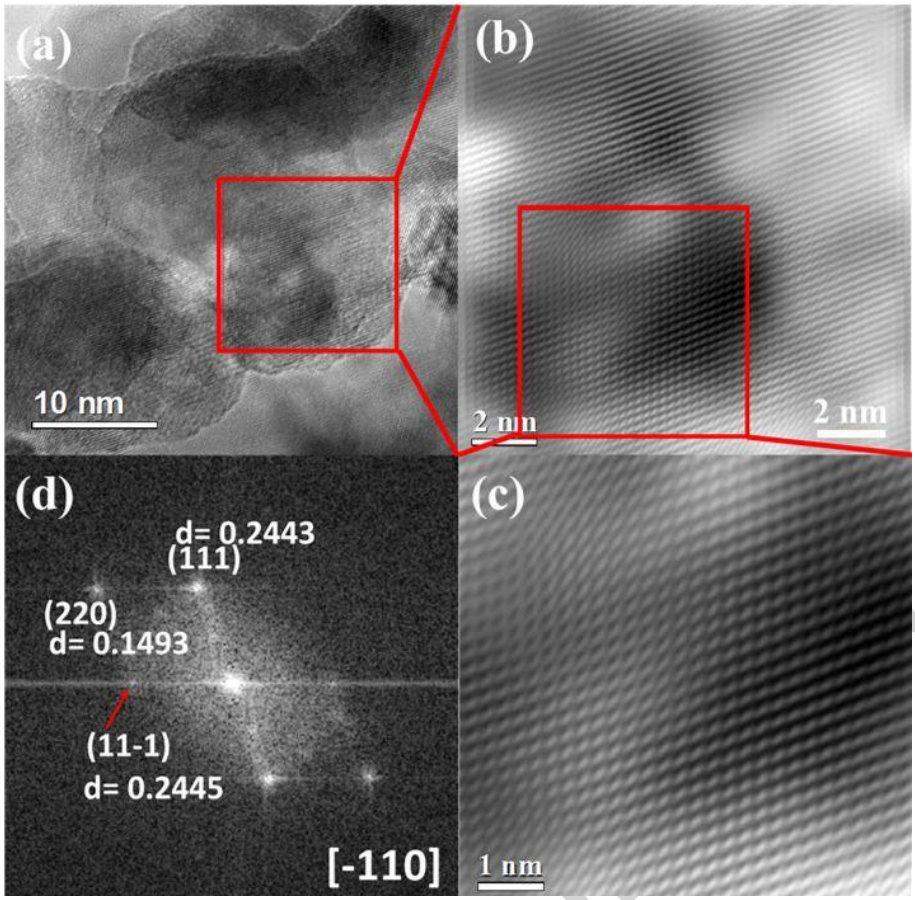

Fig. 3. The high resolution TEM image of NCO-350 (a), Fourier-filtered image (b, c) and FFT image (d) from the selected area outlined by dashed red line in (a).

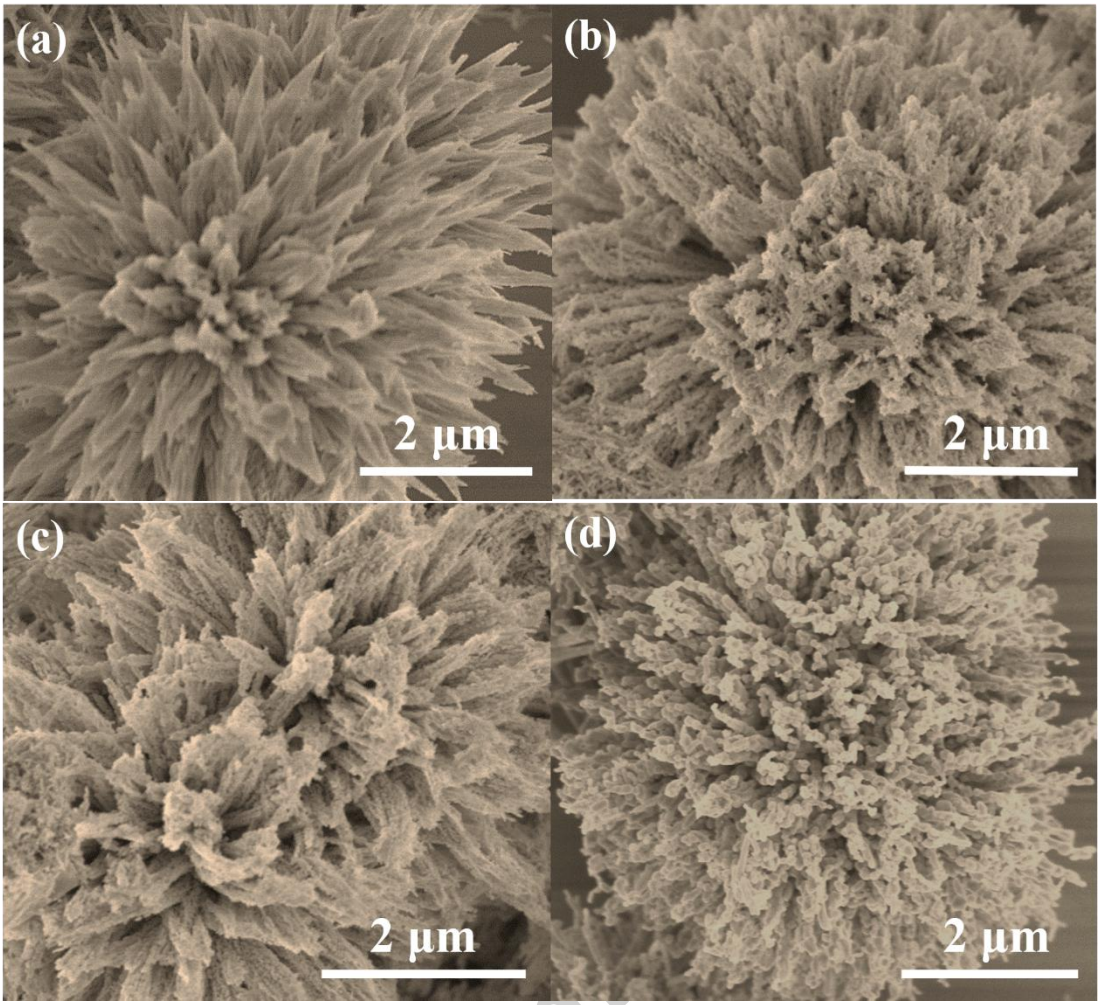

Fig. 4. The SEM images of the as-prepared NCO-350 (a), NCO-400 (b), NCO-450 (c), and NCO-500 (d), respectively.

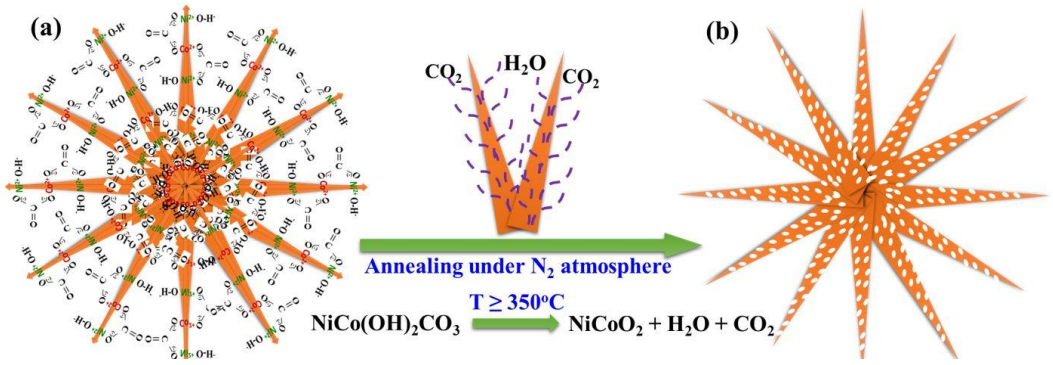

Fig. 5. The Schematic illustration of the pyrolysis process of agave-stricta-like $NiCo(OH)_2CO_3$ (a) to prepare mesoporous $NiCoO_2$ spheres (b).

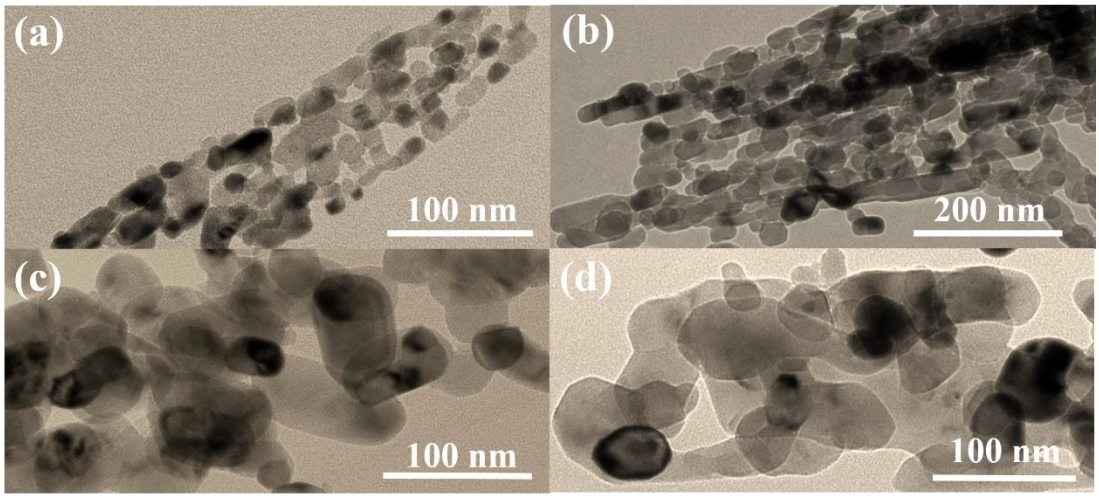

Fig. 6. The high resolution TEM images of the as-prepared NCO-350 (a), NCO-400 (b), NCO-450 (c), and NCO-500 (d), respectively.

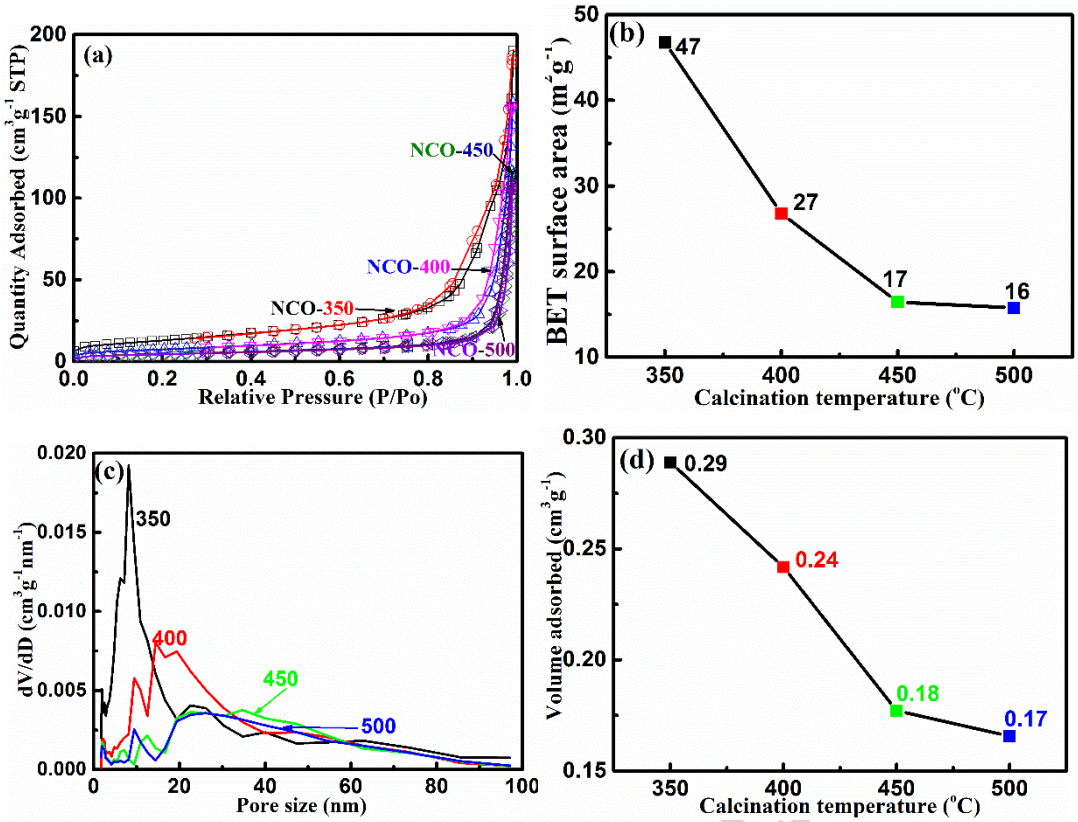

Fig. 7. The nitrogen adsorption/desorption isotherm (a) and the Brunauer–Emmett–Teller (BET) specific surface area (b) and the pore-size distribution curve (c) and the pore volume (d) of hierarchical $NiCoO_2$ mesoporous spheres varied with the calcination temperatures.

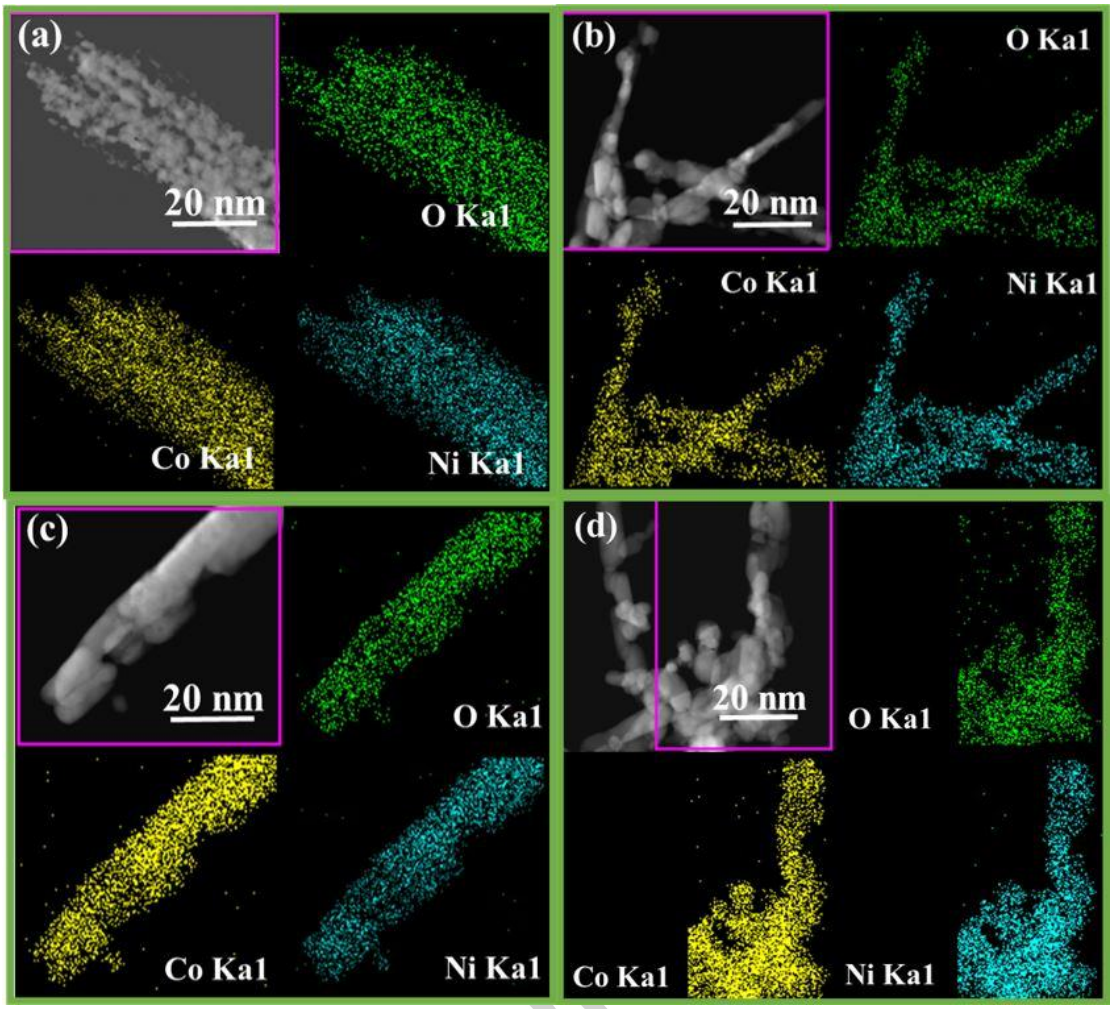

Fig. 8. FE-TEM image and corresponding EDX mapping for O, Co and Ni of NCO-350 (a), NCO-400 (b), NCO-450 (c) and NCO-500 (d), respectively.

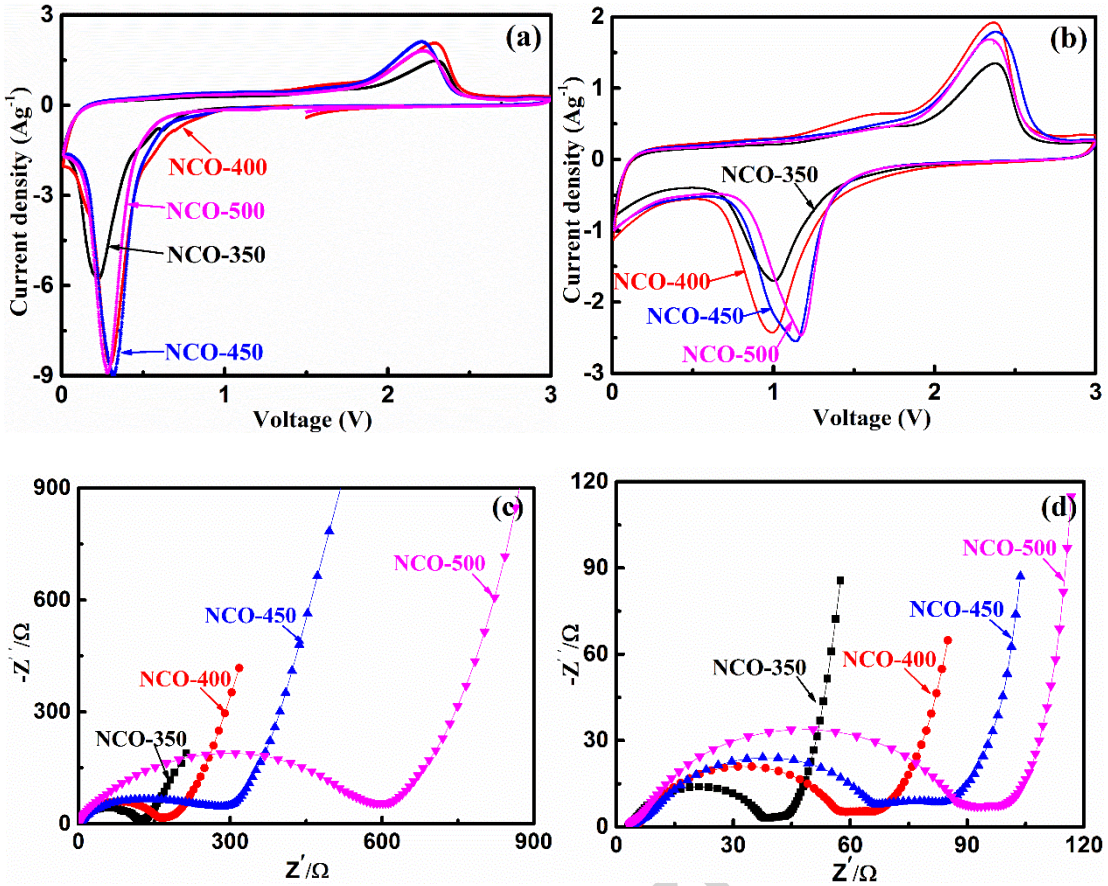

Fig. 9. The initial cycle (a) and the third cycle (b) cyclic voltammetry curve and the electrochemical impedance spectroscopy before cycle (c) and after three CV cycles (d) at 0.1 mVs^{-1} of NCO-350, NCO-400, NCO-450 and NCO-500.

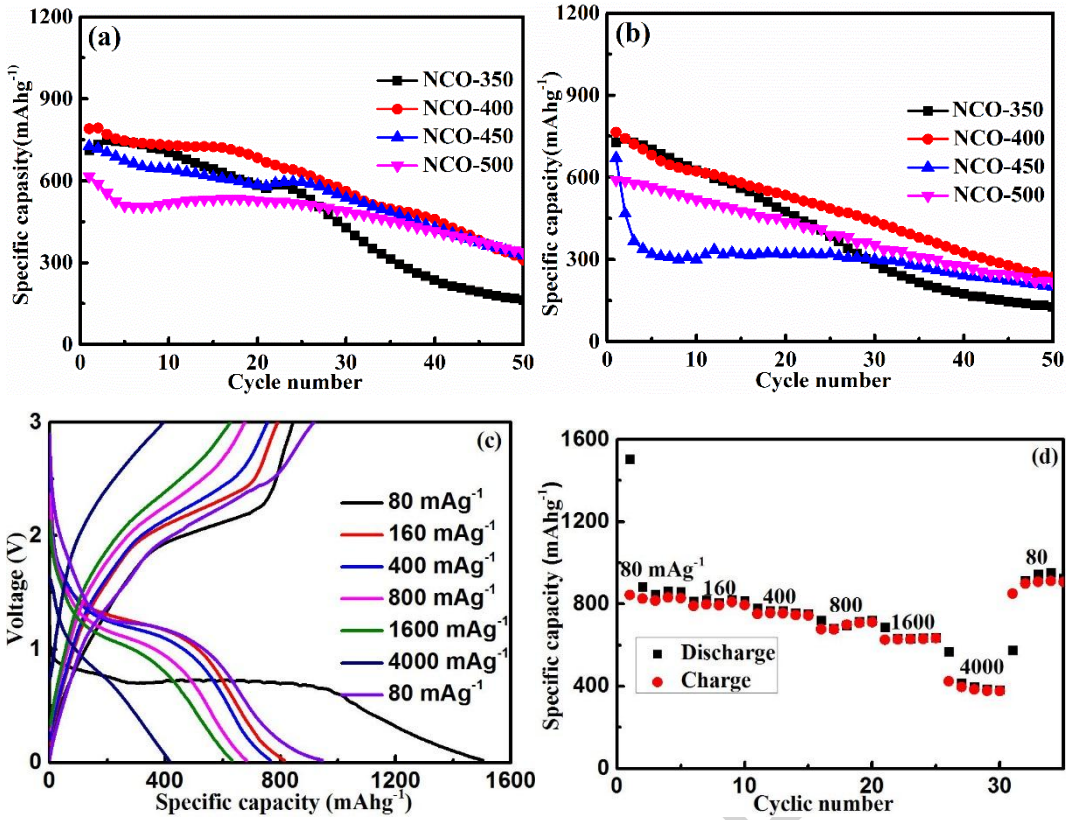

Fig. 10. The cyclic performance of NCO-350, NCO-400, NCO-450 and NCO-500 at 1600 mAg^{-1} (a) and 4000 mAg^{-1} (b); and the typical charge/discharge profile (c) and rate capability (d) of NCO-500 at the constant current densities from 80 mAg^{-1} to 4000 mAg^{-1}.

Highlights:

(1) Hierarchical $NiCoO_2$ microspheres built with mesoporous thorn arrays was successfully synthesized.

(2) The short diffusion distance and favorable active area for Li^+, together with the suppressed side reaction make $NiCoO_2$ exhibit superior rate capability and greatly promoted cyclic stability.

(3) The hierarchical microspheres structure could increase the tap density of $NiCoO_2$ in certain degree.

(4) $NiCoO_2$ with a specific surface area of 16 m^2g^{-1} could suppress the side reaction compared to NiCoO2 with larger surface area.

Graphical abstract: